

recombination in yeast (18, 19). By using an average of 12 minichunks and alternating selectable markers in each experiment, we systematically replaced the native sequence of *S. cerevisiae* III with its synIII counterpart in 11 successive rounds of transformation (Fig. 2C and table S2) (20, 21).

Genome Comparisons

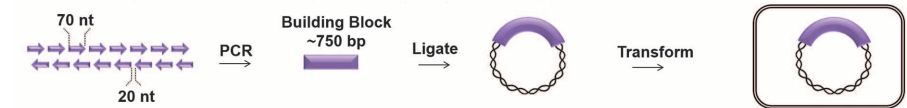
PCRTag analysis (2) revealed the presence of synIII synthetic PCRTags and absence of native PCRTags (Fig. 3A; see supplementary text and figs. S5 to S7 for the complete set of PCRTag

Fig. 2. SynIII construction. (A) BB synthesis. JHU students in the Build-A-Genome course synthesized 750-bp BBs (purple) from oligonucleotides. nt, nucleotides. (B) Assembly of minichunks. Two- to 4-kb minichunks (yellow) were assembled by homologous recombination in *S. cerevisiae* (table S1). Adjacent minichunks were designed to encode overlap of one BB to facilitate downstream assembly steps. Minichunks were flanked by a rare cutting restriction enzyme (RE) site, *Xma*I or *Not*I. (C) Direct replacement of native yeast chromosome III with pools of synthetic minichunks. Eleven iterative one-step assemblies and replacements of native genomic segments of yeast chromosome III were carried out by using pools of overlapping synthetic DNA minichunks (table S2), encoding alternating genetic markers (*LEU2* or *URA3*), which enabled complete replacement of native III with synIII in yeast.

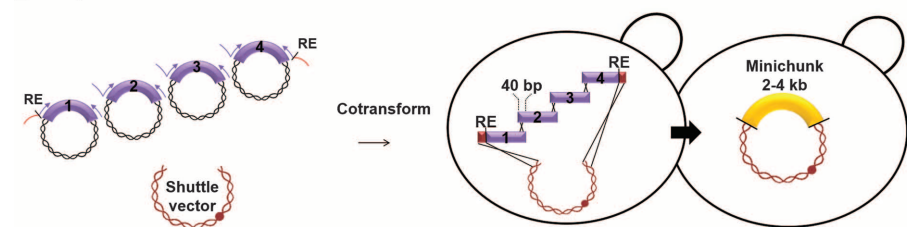
analyses). The smaller size of synIII and intermediates in its full synthesis as compared with the native yeast chromosome was demonstrated by pulsed-field gel electrophoresis (Fig. 3B and fig. S8) (22). Analysis of the intermediate strains revealed that the starting strain had some unexpected rearrangements in at least two chromosomes and that an additional rearrangement occurred during the assembly process; these did not affect synIII (fig. S8). These abnormalities were eliminated through back-crossing the synIII intermediate strain to strain BY4742 (table S3), yielding a *MAT α* strain

with an electrophoretic karyotype perfectly matching BY4742 but for the expected altered length III (compare lane 97 to 97* in fig. S8). Southern blot analyses using arm-specific radiolabeled probes further verified and validated the structure of the left- and right-arm telomere ends of synIII, which had been specified by the universal telomere cap (UTC) sequence (fig. S9). Restriction fragment sizes on Southern blots are compatible with the deletion of *HML*, *HMR*, and much of each subtelomere (fig. S9). This was further confirmed by complete genome sequencing of the synIII strain.

A Step 1: Synthesize Building Blocks (BBs) from oligonucleotides



B Step 2: Assemble 2-4 kb minichunks



C Step 3: Replace native III with minichunks

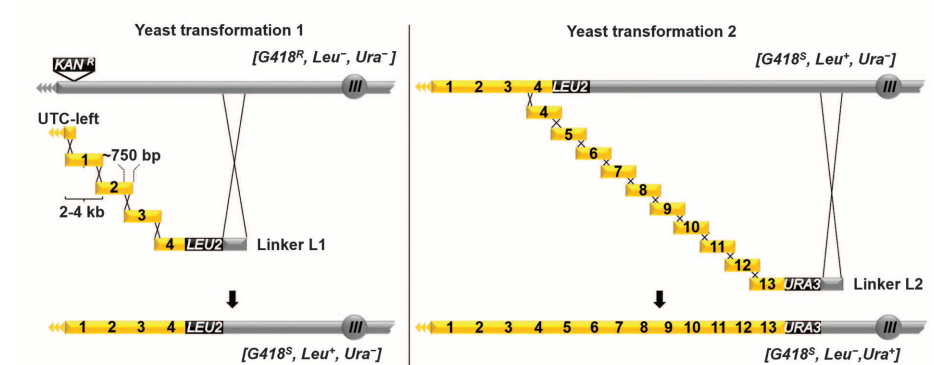
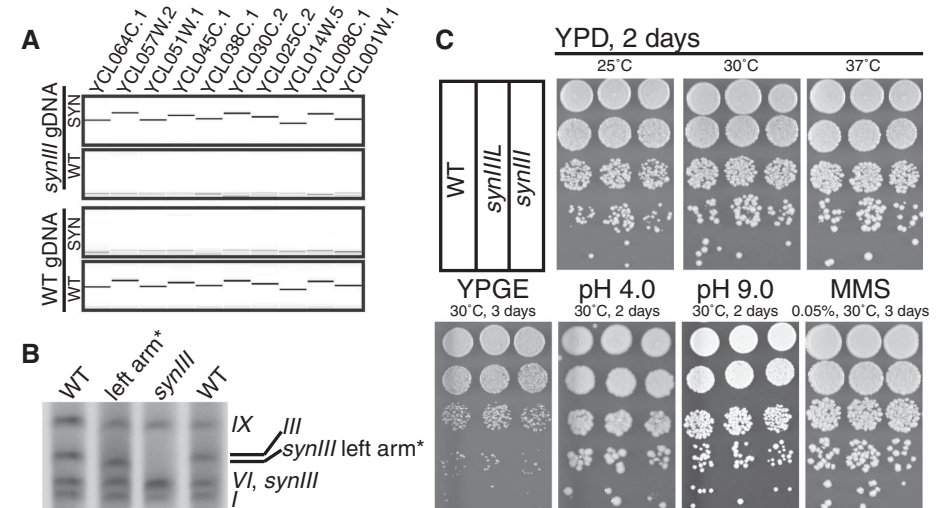


Fig. 3. Characterization and testing of synIII strain. (A) PCRTag analysis (one PCRTag per ~10 kb) of the left arm of synIII and WT yeast (BY4742) DNA is shown. Analysis of the complete set of PCRTags is shown in figs. S4 to S6. (B) Karyotypic analysis of synIII and synIIIIL strains by pulsed-field gel electrophoresis revealed the size reduction of synIII and synIIIIL compared with native III. Yeast chromosome numbers are indicated on the right side. SynIII (272,871 bp) and native chromosome VI (270,148 bp) comigrate in the gel. A karyotypic analysis of synIII and all intermediate strains is shown in fig. S8. (C) SynIII and synIIIIL phenotyping on various types of media. Tenfold serial dilutions of saturated cultures of WT (BY4742), synIIIIL, and synIII strains were plated on the indicated media and temperatures. YPD, yeast extract peptone dextrose; YPGE, yeast extract peptone glycerol ethanol; MMS, methyl methanesulfate. A complete set of synIII and synIIIIL phenotyping under various conditions is shown in fig. S11.



DNA sequencing of the *synIII* strain genome revealed sequence differences at 10 sites in *synIII* compared with our designed sequence (table S4). Nine of the changes are base substitutions or 1-bp insertions or deletions (indels). Three of the nine mutations correspond to preexisting but apparently innocuous mutations in the minichunks and BBs. Of the remainder, two correspond to the wild-type (WT) base at this position and thus may simply reflect inheritance of WT sequence. Because PCRTag analysis (table S5) was the method used to validate transformants during the 11 intermediate construction steps, the recombination events involved are patchy transformants, with tiny patches of native DNA instead of synthetic sequence that would have been missed during the PCRTag analysis. The remaining four mutations, which must have originated during the integration process, all occur in regions of overlap in the *synIII* minichunks, suggesting that the homologous recombination process may be somewhat error-prone relative to baseline error rates

(23). The tenth change is the absence of an expected *loxP*sym site.

To check for negative effects of modifications on fitness of *synIII*-containing strains from the WT (BY4742), we examined colony size, growth curves, and morphology under various conditions. A growth curve analysis established that *synIII* and the isogenic native strain had no detectable fitness difference (fig. S10). The strains were also indistinguishable from each other on colony-size tests (Fig. 3C), indicating that defects in fitness attributable to the *synIII* intermediate or *synIII* are very modest, with only 1 condition out of 21 (high sorbitol) showing a subtle fitness defect for *synIII* (fig. S11). Cell morphology of all intermediate strains was similar to that of WT (fig. S12) except that, during replacement round R3 (giving rise to strain 219 kb-*synIII*), a very low frequency (~1% of cells) of morphologically abnormal buds were observed (fig. S12). We performed transcript profiling to identify possible changes in gene expression across *synIII* or genome-wide re-

sulting from synonymous substitutions, introduction of *loxP*sym sites, and other changes. Although 10 loci are differentially expressed at genome-wide significance ($P < 7.4 \times 10^{-6}$ for 5% family-wise error rate based on 6756 loci with at least one mapped read and also corresponding to 1% false discovery rate), eight of these correspond to loci intentionally deleted from *synIII*. The remaining two loci are *HSP30* on *synIII*, ~16-fold down, and *PCL1* on native chromosome *XIV*, ~16-fold up (fig. S13).

The inclusion of hundreds of designed changes in the synthetic chromosome, including the removal of 11 transfer RNA (tRNA) genes said to be important sites of cohesin loading, might result in subtle or overt destabilizing effects on the synthetic chromosome; alternatively, removal of repetitive DNA sequences might increase stability by reducing the likelihood of “ectopic” recombination events involving two different repeat copies. Because of the 98 *loxP*sym sites added to *synIII* (and all the other changes), it was important to evaluate the genome integrity and the loss rate of the chromosome in the absence of Cre expression. PCRTag analysis revealed that *synIII* is stable over 125 mitotic generations in 30 independent lineages (Fig. 4A). To evaluate the loss rate of *synIII*, we used the a-like faker assay in which *MAT α* cells carrying *synIII* were monitored for acquiring the ability to mate as *MAT α* cells, a consequence of losing chromosome III (24). Despite the extensive chromosome engineering, the frequency of *MAT α* /*synIII* loss was not significantly different from that of the WT control (Fig. 4B).

It is not known whether cohesin accumulation at a tRNA gene region directly depends on the presence of the tRNA gene, nor is its effect on chromosome stability clear. We compared the map of cohesin binding sites on native chromosome III and *synIII* by using chromatin immunoprecipitation sequence (ChIP-seq) analysis (fig. S14). The overall cohesin binding pattern is similar between the two chromosomes. However, at three tRNA genes that show a prominent peak in the native chromosome, that peak is reduced or in one case [the glutamine tRNA gene tQ(UUG)C] completely absent from *synIII* (fig. S14). Thus, we conclude that tRNA genes and their documented interactions with both cohesin and condensin (25, 26) are dispensable for high levels of chromosome stability. We also compared the replication dynamics of *synIII* and native III (supplementary text, table S9, and fig. S15) and saw few dramatic changes in dynamics in spite of several autonomously replicating sequences having been deleted.

SCRaMBLEing in haploid strains containing chromosome *synIII* leads to lethality via essential gene loss (fig. S16). We looked for more subtle effects of SCRaMBLE in a heterozygous *MAT α* /*synIII* (mating incompetent) diploid strain with a synthetic *MAT α* chromosome and a native *MAT α* chromosome *synIII*/III; (fig. S17). We introduced the Cre-EBD plasmid into such strains, as well as into

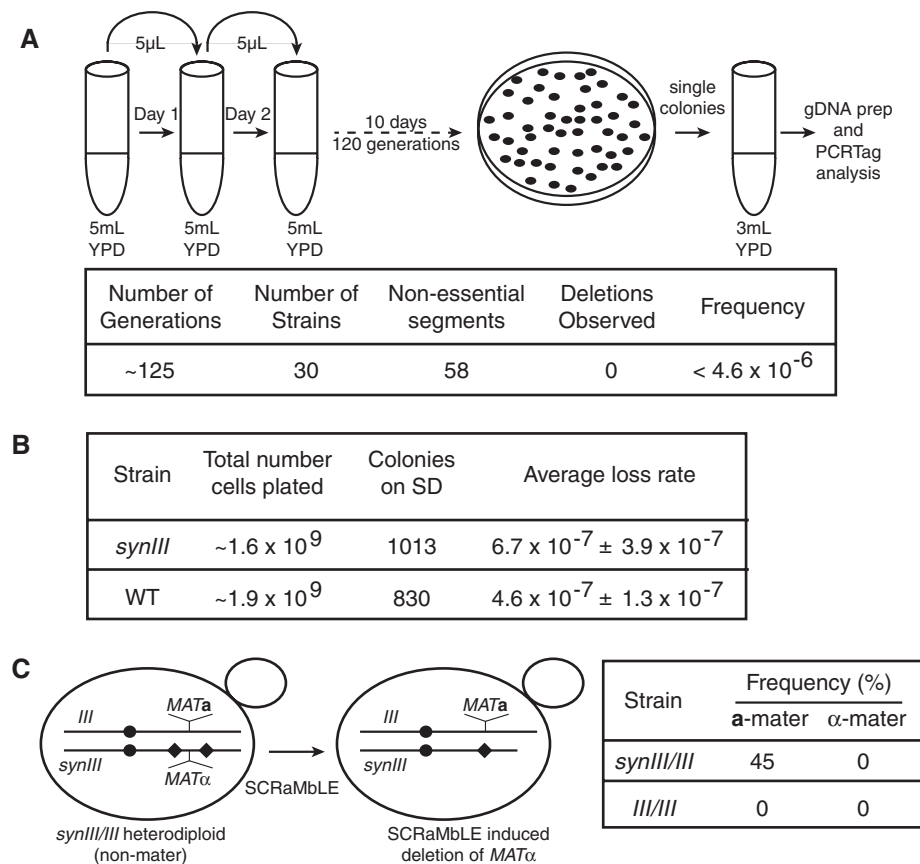


Fig. 4. Genomic stability of the *synIII* strain. (A) PCRTag analysis of *synIII* strain after ~125 generations. We assayed for the loss of 58 different segments lacking essential genes in the absence of SCRaMBLEing; no losses were observed after over 200,000 segment-generations analyzed; reported frequency is a maximum estimate of segment loss frequency per generation. gDNA, genomic DNA. (B) Evaluation of the loss rate of *synIII* chromosome using a-like faker assay. No significant change in the loss frequency was observed, although the absolute loss rate value is modestly higher in *synIII*. SD, standard dextrose. (C) SCRaMBLE leads to a gain of mating type a behavior in *synIII* heterozygous diploids. Frequencies are of a-mater and α -mater colonies post-SCRaMBLE (induction with estradiol) in *synIII*/III and III/III strains. A complete SCRaMBLE analysis is shown in fig. S18. Diamonds represent *loxP*sym sites, and circles indicate centromeres.

WT *MATa/α* diploids (III/III), and very briefly induced with estradiol. In spite of the minimal level of SCRaMbLEing induced, we observed a massive increase in the frequency of a-mater derivatives in the native III/synIII heterozygous strains (Fig. 4C and fig. S18). Such a-mater derivatives can arise from the loss of the *MATa* locus, because such *MAT*-less strains express a-specific genes. PCRTag mapping of several such derivatives showed that these variants had indeed lost different sections of synIII, all of which included the *MAT* locus (fig. S18).

The total synthesis of the synIII chromosome represents a major step toward the design and complete synthesis of a novel eukaryotic genome structure using the model *S. cerevisiae* as the basis for a synthetic designer genome, Sc2.0. The many changes made to synIII, including intron deletion, tRNA gene removal, and loxP sites and PCRTags introduction, do not appear to significantly decrease the fitness or alter the transcriptome or the replication timing of the synIII strain, supporting the very pliable nature of the yeast genome and potentially allowing for much more aggressively redesigned future genome versions. Sc2.0 represents just one of myriad possible arbitrary genome designs, and we anticipate that synthetic chromosome design will become a new means of posing specific evolutionary and mechanistic questions about genome structure and function. Rapid advances in synthetic biology coupled with ever decreasing costs of DNA synthesis suggest that it will soon become feasible to engineer new eukaryotic genomes, including plant and animal genomes, with synthetic chromosomes encoding desired functions and phenotypic properties based on specific design principles.

References and Notes

1. A. Goffeau *et al.*, *Science* **274**, 546–567 (1996).
2. J. S. Dymond *et al.*, *Nature* **477**, 471–476 (2011).
3. J. Dymond, J. Boeke, *Bioeng. Bugs* **3**, 168–171 (2012).
4. J. Cello, A. V. Paul, E. Wimmer, *Science* **297**, 1016–1018 (2002).
5. L. Y. Chan, S. Kosuri, D. Endy, *Mol. Syst. Biol.* **1**, 0018 (2005).
6. G. Pósfai *et al.*, *Science* **312**, 1044–1046 (2006).
7. D. G. Gibson *et al.*, *Science* **319**, 1215–1220 (2008).
8. C. Lartigue *et al.*, *Science* **317**, 632–638 (2007).
9. H. H. Wang *et al.*, *Nature* **460**, 894–898 (2009).
10. D. G. Gibson *et al.*, *Science* **329**, 52–56 (2010).
11. F. J. Isaacs *et al.*, *Science* **333**, 348–353 (2011).
12. S. G. Oliver *et al.*, *Nature* **357**, 38–46 (1992).
13. S. M. Richardson, S. J. Wheelan, R. M. Yarrington, J. D. Boeke, *Genome Res.* **16**, 550–556 (2006).
14. W. P. Stemmer, A. Cramer, K. D. Ha, T. M. Brennan, H. L. Heyneker, *Gene* **164**, 49–53 (1995).
15. J. S. Dymond *et al.*, *Genetics* **181**, 13–21 (2009).
16. N. Annaluru *et al.*, *Methods Mol. Biol.* **852**, 77–95 (2012).
17. D. G. Gibson *et al.*, *Nat. Methods* **6**, 343–345 (2009).
18. H. Ma, S. Kunes, P. J. Schatz, D. Botstein, *Gene* **58**, 201–216 (1987).
19. V. Larionov *et al.*, *Proc. Natl. Acad. Sci. U.S.A.* **93**, 491–496 (1996).
20. D. G. Gibson *et al.*, *Proc. Natl. Acad. Sci. U.S.A.* **105**, 20404–20409 (2008).
21. H. Muller *et al.*, *Methods Mol. Biol.* **852**, 133–150 (2012).
22. D. C. Schwartz, C. R. Cantor, *Cell* **37**, 67–75 (1984).
23. M. Lynch *et al.*, *Proc. Natl. Acad. Sci. U.S.A.* **105**, 9272–9277 (2008).
24. K. W. Yuen *et al.*, *Proc. Natl. Acad. Sci. U.S.A.* **104**, 3925–3930 (2007).
25. C. D'Ambrosio *et al.*, *Genes Dev.* **22**, 2215–2227 (2008).
26. A. Lengronne *et al.*, *Nature* **430**, 573–578 (2004).

Acknowledgments: This work was supported by grants from NSF (MCB 0718846) to J.D.B., J.S.B., and S.C. and from Microsoft to J.S.B. S.M. and S.C. were supported by a grant from NIH (GM077291 to S.C.); H. Muller, by a fellowship from Fondation pour la Recherche Médicale and a Pasteur-Roux fellowship; S.R., by an Exploratory Research Grant from the

Maryland Stem Cell Research Fund; L.A.M., by a fellowship from the National Sciences and Engineering Research Council of Canada; S.M.R., by a fellowship from the U.S. Department of Energy; and J.S.D., by a fellowship from JHU Applied Physics Laboratory. We thank D. Gibson for helpful suggestions regarding the isothermal assembly reaction, E. Louis and D. Gottschling for advice on synthetic telomere design, and L. Teytelman and J. Rine for advice on silent cassette DNA. The synIII sequences have been deposited at GenBank with accession numbers KJ463385 (the as-designed reference sequence version 3.3_41) and KC880027 (the actual physical sequence in strain HMSY011, sequence version 3.3_42). The authors declare no competing financial interests. Requests for materials should be addressed to J.D.B. (boekej01@nyumc.org). We dedicate this publication to the memory of Har Gobind Khorana, who synthesized the first yeast tRNA gene. N. Annaluru, H. Muller, J.S.B., J.D.B., and S.C. designed experiments. J.D.B. and S.M.R. designed synIII. N. Annaluru, H.M., L.A.M., S.R., G.S., S.M.R., J.S.D., Z.K., Y.C., Z.G., V.L., S.M., K.K., N. Agmon, G.F., and S.C. performed experiments. N. Annaluru, H.M., G.S., R.K., J.D.B., and S.C. analyzed data. N. Annaluru, H.M., J.D.B., and S.C. wrote the manuscript. JHU Build-A-Genome course students (K. Caravelli, K. Cirelli, Z.G., V.L., A.Y., M.B., P.B., K.M.B., B.J.C., J.C., K. Charoen, W.J.C., P.D., J.E.D., J. Doong, J. Dunn, J.I.F., C.F., C.E.F., D.G., P.H., I.I., J.J., C.Y.L.L., P.A.L., S.L., D.L., M.E.L., J. Ling, Jaime Liu, Jonathan Liu, M.L., H.Ma, J.M., J.E.M., A.M., A.M.M., W.C.O., Y.O., R.P., M.P., L.C.P., J.Q., A.R., M.G.R., I.Y.S., N.E.S., V.S., A.S., A.W., R.W., W.R.X., Y.X., A.T.Y.) synthesized most of the building blocks for synIII; H. Muller, G.S., S.M.R., J.S.D., L.Z.S., E.M.C., Y.C., K.Z., J.S.H., M.H., J.T. and J.D.B. taught the Build-A-Genome course. S.C. led the effort on the construction and assembly of synIII.

Supplementary Materials

www.sciencemag.org/content/344/6179/55/suppl/DC1
Materials and Methods

Supplementary Text

Fig. S1

Table S1

References (27–48)

3 December 2013; accepted 6 March 2014

Published online 27 March 2014;

10.1126/science.1249252

Structure of a Class C GPCR Metabotropic Glutamate Receptor 1 Bound to an Allosteric Modulator

Huixian Wu,^{1*} Chong Wang,^{1*} Karen J. Gregory,^{2,3} Gye Won Han,¹ Hyekyung P. Cho,² Yan Xia,⁴ Colleen M. Niswender,² Vsevolod Katritch,¹ Jens Meiler,⁴ Vadim Cherezov,¹ P. Jeffrey Conn,² Raymond C. Stevens^{1†}

The excitatory neurotransmitter glutamate induces modulatory actions via the metabotropic glutamate receptors (mGlu), which are class C G protein-coupled receptors (GPCRs). We determined the structure of the human mGlu₁ receptor seven-transmembrane (7TM) domain bound to a negative allosteric modulator, FITM, at a resolution of 2.8 angstroms. The modulator binding site partially overlaps with the orthosteric binding sites of class A GPCRs but is more restricted than most other GPCRs. We observed a parallel 7TM dimer mediated by cholesterol, which suggests that signaling initiated by glutamate's interaction with the extracellular domain might be mediated via 7TM interactions within the full-length receptor dimer. A combination of crystallography, structure-activity relationships, mutagenesis, and full-length dimer modeling provides insights about the allosteric modulation and activation mechanism of class C GPCRs.

The human G protein-coupled receptor (GPCR) superfamily comprises more than 800 seven-transmembrane (7TM) receptors that can be divided into four classes accord-

ing to their sequence homology: class A, B, C, and F (Frizzled) (*1*). Class C GPCRs play important roles in many physiological processes such as synaptic transmission, taste sensation, and cal-

cium homeostasis; they include metabotropic glutamate receptors (mGlu), γ -aminobutyric acid B (GABA_B) receptors, calcium-sensing (CaS) receptors, and taste 1 (TAS1) receptors, as well as a few orphan receptors. A distinguishing feature of class C GPCRs is constitutive homo- or heterodimerization mediated by a large N-terminal extracellular domain (ECD) (Fig. 1A). The ECDs within homodimeric receptors (mGlu and CaS) are cross-linked via an intermolecular disulfide bond. The heterodimeric receptors (GABA_B and TAS1) are not covalently linked, but their heterodimerization is required for trafficking to the cell surface and signaling (*2*). The ECD of class C

¹Department of Integrative Structural and Computational Biology, The Scripps Research Institute, 10550 North Torrey Pines Road, La Jolla, CA 92037, USA. ²Department of Pharmacology and Vanderbilt Center for Neuroscience Drug Discovery, Vanderbilt University Medical Center, Nashville, TN 37232, USA. ³Drug Discovery Biology, Monash Institute of Pharmaceutical Sciences, Monash University, Parkville, Victoria, Australia. ⁴Center for Structural Biology and Department of Chemistry and Institute for Chemical Biology, Vanderbilt University Medical Center, Nashville, TN 37232, USA.

*These authors contributed equally to this work.

†Corresponding author. E-mail: stevens@scripps.edu